160159871

Thermal Modelling & Temperature Prediction of a Power Module Mounted on an IMS PCB

Benjamin James Griffiths

Abstract – **This paper describes the process of characterising and modelling the thermal behaviour of a H-Bridge power module containing four MOSFET devices mounted onto an insulated metal substrate PCB. The temperature elevation of a device due to a known power dissipation can be determined using its transient thermal impedance. Since there are multiple heat-generating devices on the board, the temperature elevation of each device is due to their own self-heating as well as the effects of thermal cross-coupling between other devices. The transient thermal behaviour of the system can be modelled using a compact electrical RC network, which is derived by performing a step change in power dissipation and observing the temperature elevation, and can be implemented in a circuit simulator such as LTSpice. The thermal model produced can be used to predict the temperature of each device due to any combination of power dissipation in each device. There is good agreement between the modelled and measured temperature elevation when the devices are subjected to different power dissipation waveforms.**

I. INTRODUCTION

There is an increasing demand for power electronics that offer greater power capabilities whilst maintaining a smaller physical footprint, especially in recent times with the rapid development of electric vehicles, where power electronics are often subjected to challenging size constraints, complicating thermal management. [1][2] The ability to precisely model the thermal behaviour of a power module is necessary to ensure the devices do not exceed their rated operating conditions, thus improving device reliability and operational lifetime, whilst reducing failure rate. In the context of power modules in electric vehicles that drive the powertrain, the wide range of operating conditions that arise from driver inputs can cause high operating temperatures and rapid thermal cycling, which can result in failures in solder joints and bond wires inside semiconductor packages due to mechanical stresses. By having the ability to model and predict the temperature of the system under different load conditions, power throttling or active cooling can be implemented to keep the system within a desired temperature range, and information can be used in conjunction with degradation models to predict operational life-time. [3] Furthermore, by using a correction observer with the model, is it possible to determine the temperature elevation of multiple individual devices using only a few temperature sensors to correct the model when there are changes in operating conditions. This is especially useful in electric vehicle power modules that often contain hundreds of switching devices, where it would be expensive and unpractical to mount temperature sensors to individual devices.

This 3rd year Individual Project was performed at the Department of Electronic & Electrical Engineering at the University of Sheffield, UK It was supervised by Martin Foster (e-mail: M.P.Foster@sheffield.ac.uk).

This paper focusses on deriving a thermal model for a simple H-Bridge power module shown in figure 1, consisting of four MOSFETs mounted onto an insulated metal substrate (IMS) printed circuit board, which is manufactured by printing the circuit onto a sheet of aluminium, separated by a thin electrically isolating layer. This printed circuit board structure provides superior heatsinking performance for surface mount components compared to traditional types.

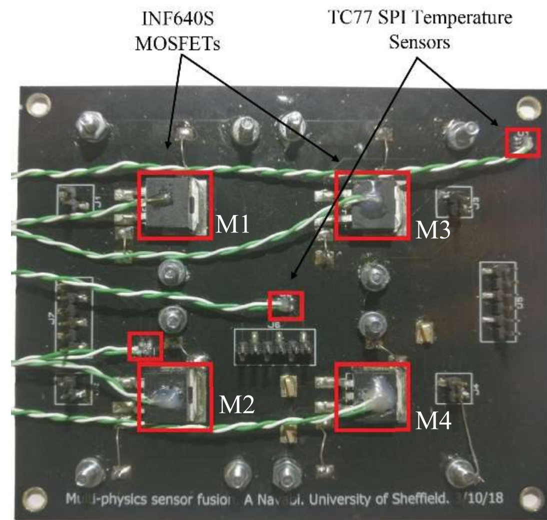

Figure 1: Insulated metal substrate PCB.

By performing temperature measurements at various points on the circuit in response to a devices power dissipation, a model can be produced that allows the temperature of each device to be predicted for any given combination of device power dissipation.

Conventionally, the steady-state thermal resistance of a device is given on its data sheet, and can be used to calculate the required heatsink value to keep the device at a certain temperature for a given power dissipation. However, this only describes the maximum temperature that the device is able to reach, and assumes it reaches that temperature instantaneously, when in reality, it takes a finite time for devices to reach steady state temperature. In order to accurately predict the temperature of a system, a way of modelling the transient thermal behaviour is required. This can be accounted for by using a complex thermal impedance instead, using resistors and capacitors as electrical analogues for steady state thermal resistance and heat capacity respectively. Furthermore, since there are multiple devices within close proximity to one another on the board, the temperature elevation of a device is not only due to its own self-heating, but is also due to the self-heating from nearby devices, known as thermal cross coupling. Without taking the thermal cross coupling effects into consideration, the model may lead to an underestimate of a device's temperature.

Electrical equivalent thermal models are used due to their simplicity and ability to be modelled using readily available circuit simulators such as LTSpice. The two main types of RC networks commonly used in thermal modelling are the Foster network and the Cauer network, as seen in figure 2. In these circuit diagrams, the heat dissipation is modelled as a current source, which gives rise to a voltage (analogous to temperature) across each section of the circuit. [4]

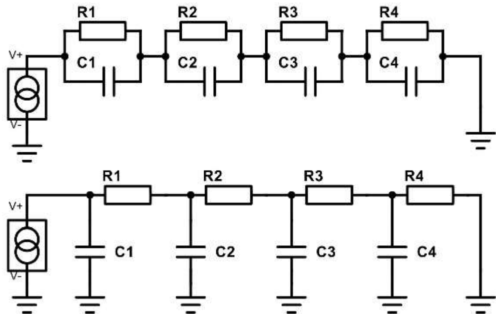

Figure 2: Foster network (top) and Cauer network (bottom).

The Foster network contains multiple parallel RC combinations connected end to end, where the time constant of each section can be extracted from a multi-term exponential equation. However, since the Foster network is simply a representation of the time constants within a system, only the end nodes have any physical significance, being the ambient temperature (ground) and the junction temperature. This is because the model is not based upon the physical material properties of the system, rather it is designed from the systems thermal step response.

On the other hand, each section in the Cauer networks has their capacitor voltage referenced to ground, hence each node in the network has physical significance and represents a real temperature with respect to ambient within the system. These networks can be used to model temperatures at different physical layers within a device, such as the layers between a semiconductor die and the surface of the circuit board.

Since the only temperatures we are concerned with in this paper are the temperatures of the individual devices, a Foster network is suitable due to the ability to extract the resistor and capacitor values using experimental step response data.

There are several methods that can be used to measure the temperature of devices on a circuit board. A common approach is to use a K-type thermocouple attached to the body of a device using a thermal epoxy. Thermocouples operate by producing a small voltage across the terminals of the device proportional to the temperature experience at the coupling, typically around 37 µV/°C. The advantages of using thermocouples are their fast response time, low cost and wide availability. However, they require expensive and complex electronics due to the small voltages involved and the noise suppression required to obtain precise temperature measurements. Another problem with using thermocouples to measure the temperature of semiconductor devices is that they can cannot be mounted directly onto the semiconductor die, rather they have to be mounted externally onto the device's plastic packaging. This effectively introduces an internal thermal impedance between the heat generating semiconductor die, and the temperature sensor, giving rise to a time delay before the temperature of the die is detected by the sensor. In certain circumstances, this could result in a large temperature error between the actual die temperature and what the sensor reads, potentially leading the device to exceed safe operation conditions unintentionally. Therefore, to properly understand the temperature of the devices on the circuit board, a non-intrusive method to measure the temperature of the semiconductor die is required.

Many semiconductor junctions possess an electro-thermal relationship, and in the case of the MOSFET devices on the power module, there is a voltage-temperature relationship in the internal anti-parallel/body diode, an intrinsic feature of the devices structure. [5]

$$V_d = \frac{kT}{e} \ln\left(\frac{I}{I_s} - 1\right) \tag{1}$$

By analysing (1), it can be seen that if the current I, is kept constant, there is a direct relationship between the forward bias voltage V_d and the temperature T. Therefore, by injecting a constant bias current into the source of the MOSFET, with the gate grounded so current only flows through the body diode, the voltage developed between the drain and source can be measured and related to the die temperature.

Within the normal operating temperature range of the MOSFETs, this relationship is approximately linear, hence the relationship can be described using (2).

$$V_d = m \cdot T_j + V_0 \tag{2}$$

Terms m and V_0 are the gradient and intercept of the relationship respectively, which are determined experimentally.

II. ECONOMIC, LEGAL, SOCIAL AND ENVIRONMENTAL CONTEXT

With stricter regulations around vehicle emissions, and with more renewable energy sources being used in the grid, electric vehicles are being developed due to their lower environmental impact. This project is related to the development of electric vehicles, and in particular, the reliability and longevity of their power electronics.

The impact that this research may have include increasing the service life of an electric vehicles power electronics, and reducing the likelihood of thermally related failures. This may improve vehicle safety, and reduces electronic waste as a result of a reduced failure rate.

Furthermore, from a vehicle manufacturers perspective, there could be economic benefits from reduced chances of vehicle repairs or a recall. This could also improve public perception relating to the produce reliability of a certain brand or electric vehicles in general.

III. METHODOLOGY

The diagram in figure 3 shows the process of thermally characterising the power module and developing a suitable model.

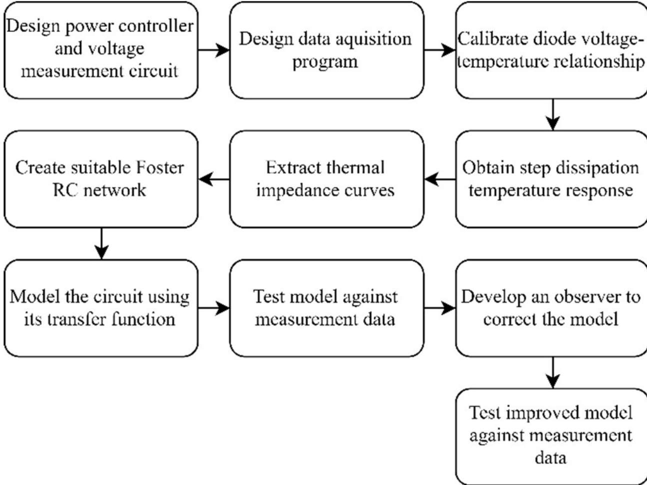

Figure 3: Project structure flow diagram.

The first step was to design a power controller circuit that allows the power dissipation in any of the devices to be precisely controlled, shown in figure 4.

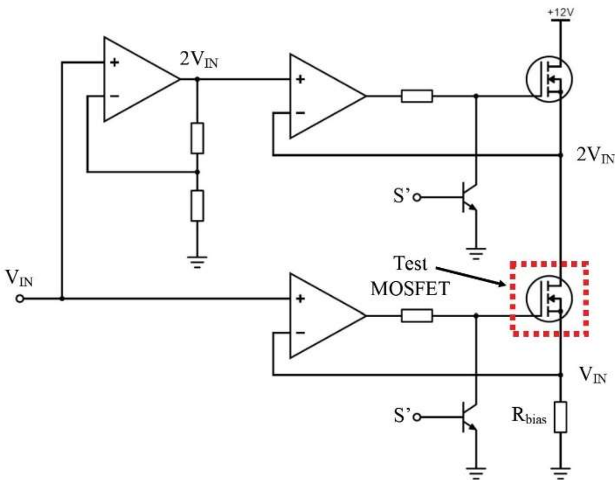

Figure 4: Power controller circuit schematic.

This circuit contains a constant current driver and uses negative feedback to maintain the input voltage V_{IN} across the bias resistor R_{bias}, and $2V_{IN}$ at the drain of the test MOSFET. Therefore, V_{IN} is also maintained across the test MOSFET terminals, which allows the power dissipation to be controlled with a suitable combination of R_{bias} and V_{IN}. The switches, labeled as S', allow the circuit to be turned off by pulling the gates of the MOSFETs to ground. [7]

The next part of the circuit is responsible for measuring the voltage developed across the MOSFET body diode when a small bias current is injected into the source. Due to the bias current flowing in the opposite direction to the power controller current, the voltage measurement circuit must operate on an isolated supply.

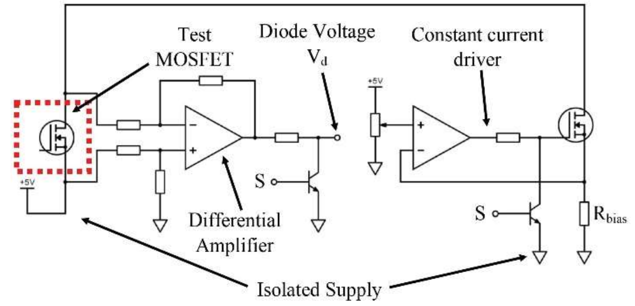

Figure 5: Voltage measurement circuit schematic.

The circuit in figure 5 shows the voltage measurement circuit, with the test MOSFETs body diode being connected to an isolated supply through a constant current driver. The bias resistor R_{bias} can be chosen to set a constant bias current for a given input voltage at the non-inverting input of the operational amplifier. The differential amplifier amplifies the difference between the source and drain to output the diode voltage. Similar to the power controller circuit, the switches allow for the constant current driver to be turned off, and the output of the differential amplifier to be pulled to ground to protect the ADC from voltages that may exceed its ratings while the power controller is operating.

In order to achieve simultaneous power dissipation and diode voltage measurement, the power controller circuit needs to momentarily turned off for a short time to the diode voltage can be measured. A PWM style scheme can be used to achieve this as seen in figure 6.

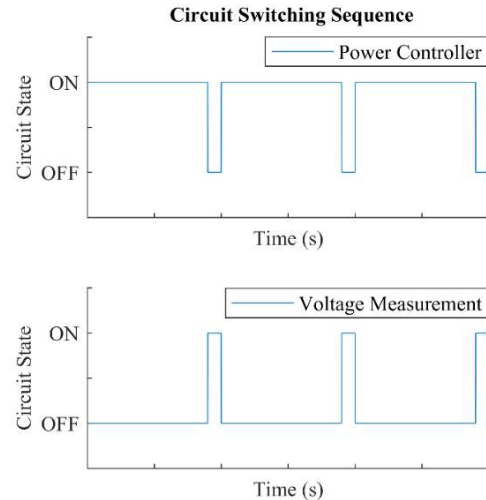

Figure 6: Circuit switching sequence example.

As long as the active duration of the measurement circuit is low compared to the duration of power dissipation, near-simultaneous power dissipation and diode voltage measurements are possible with minimal reduction to the average power dissipation. In certain circumstances, where a specific average power dissipation is required, the power can be increased slightly to take the voltage measurement time period into account.

The final circuit board that includes both the power controller and the voltage measurement functions is shown in figure 7.

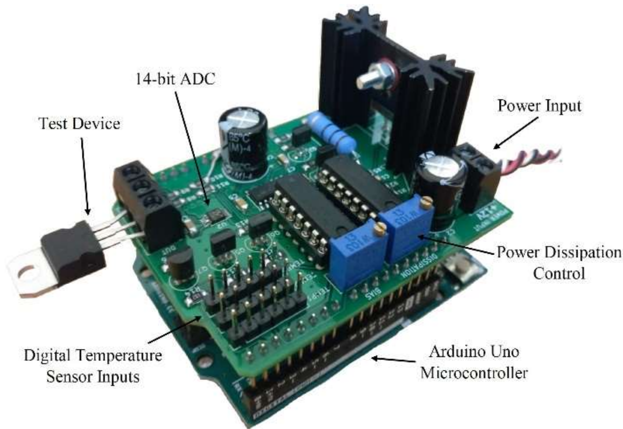

Figure 7: Full circuit on an Arduino Uno 'shield'.

The circuit can be connected directly to a readily available Arduino Uno, which is responsible for controlling the circuits functions and extracting temperature data to be sent to the data acquisition program.

The next step was to design a data acquisition program that can communicate with the Arduino Uno to access all the temperature data from the thermocouples, digital temperature sensors and the diode voltage, while having the ability to switch between power dissipation and voltage measurement modes. A LabVIEW program was created to perform these tasks, which could display all the temperature readings on a graph and export all the data to an Excel spreadsheet for later processing, shown in Appendix Figure 1 & 2.

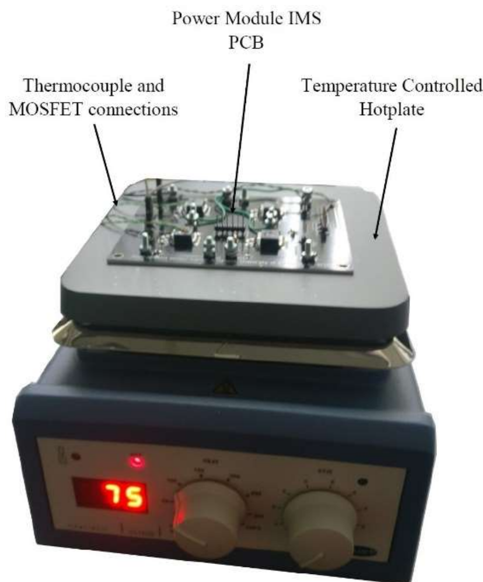

Figure 8: Calibration experiment apparatus.

In order to establish the relationship between the diode voltage and temperature, the devices needed to be subjected to incremental temperature changes, and have their diode voltages measured. To achieve this, the IMS PCB was placed onto a temperature-controlled hotplate, seen in figure 8, and thermocouples were placed on the case of each device. At each temperature increment, a settling time was given to allow the heat flux the saturate the entire device before reading the diode voltage. This was to ensure the temperature of the thermocouple was in equilibrium with to the semiconductor die temperature. The LabVIEW programs graph was used to visually confirm the device was at thermal equilibrium before taking the voltage readings. Using the data acquired, the gradient and intercept of the relationship was determined and was entered into the LabVIEW program, allowing the die temperature to be graphed and compared to the other sensors.

With the required temperature sensors attached and control circuitry complete, the transient thermal impedance can be measured experimentally. This is done by applying a step change in power dissipation to a device on the board, and measuring the temperature elevation of all of the devices.

Since the Foster network is comprised of several parallel RC pairs, each with their own time constant, the transient thermal impedance between each device can be modelled using the exponential curve obtained from step response data. The step response is modelled with zero-initial conditions so that it produces the temperature rise above ambient of the devices.

The transient thermal impedance is calculated from the step response data by subtracting the ambient temperature T_a from the junction temperature T_j, and dividing by the power dissipation in the device, shown in (3).

$$Z_{TH}(t) = \frac{T_j(t) - T_a(t)}{P} \tag{3}$$

Next, to extract the required RC component values in the Foster network to model the transient thermal impedance curve, the curve fitting tool in MATLAB was used to fit the curve to a multi-term exponential equation, shown in (4), where R_n and C_n are the resistor and capacitor values of each parallel RC pair respectively. [8]

$$Z_{TH}(t) = \sum_{n=1}^{N} R_n \left[(1 - \exp\left(-\frac{t}{R_n C_n}\right) \right] \tag{4}$$

The curve fitting procedure was repeated for all the thermal impedances between all the devices.

To model the temperature elevation of a device on the board due to the self-heating of any device, the transfer function of each Foster network was determined, with a two-term example shown in (5).

$$Z_{TH}(s) = \frac{R_1}{1 + sR_1C_1} + \frac{R_2}{1 + sR_2C_2} \tag{5}$$

As previously described, the temperature elevation of a device is due to both the self-heating of that device, and its thermal cross-coupling between other devices. Hence, by performing a linear superposition of the contributions of each heat source on the board, the total temperature elevation of a device can be calculated.

This can be conveniently represented in matrix form as seen in (6), where $T_{j1} - T_{j4}$ and $P_1 - P_4$ are the temperatures and power dissipations of each MOSFET respectively, and T_a is the ambient temperature. The transfer function of each transient thermal impedance is entered into a 4x4 matrix, where the diagonal terms are the self-heating impedances, and the vertical and horizontal terms are the thermal cross-coupling impedances. For example, Z_{11} represents the self-heating of device 1 due to the heating of device one. On the other hand, Z_{21}, Z_{31} and Z_{41} represent the thermal cross-coupling between device 1 and devices 2,3,4 due to the heating of device 1. [9]

$$\begin{bmatrix} T_{j1} \\ T_{j2} \\ T_{j3} \\ T_{j4} \end{bmatrix} = \begin{bmatrix} T_a \\ T_a \\ T_a \\ T_a \end{bmatrix} + \left(\begin{bmatrix} Z_{11} & Z_{12} & Z_{13} & Z_{14} \\ Z_{21} & Z_{22} & Z_{23} & Z_{24} \\ Z_{31} & Z_{32} & Z_{33} & Z_{34} \\ Z_{41} & Z_{42} & Z_{43} & Z_{44} \end{bmatrix} \times \begin{bmatrix} P_1 \\ P_2 \\ P_3 \\ P_4 \end{bmatrix} \right) \quad (6)$$

Therefore, as an example, the temperature of device 1 can be described in the Laplace domain using (7).

$$T_{j1} = T_a + P_1 Z_{11} + P_2 Z_{12} + P_3 Z_{13} + P_4 Z_{14} \quad (7)$$

Using the temperature elevation equations for each device, the model was then tested against actual measurements in the time-domain. This was done by dissipating a square wave waveform in a device on the board, with a variable frequency and duty cycle. The temperature curve produced was compared to the measured temperatures to assess the accuracy of the model.

IV. RESULTS & EVALUATION

The first set of experimental data obtained was the relationship between the diode voltage and temperature, which was obtained by placing the IMS PCB onto a temperature-controlled hotplate and measuring the diode-voltage of each MOSFET at each temperature increment. This experiment was performed in temperature increments of 5° from 30° - 100°. At each temperature increment, the connections to the voltage measurement circuit were attached to each MOSFET in turn, and diode voltage measurements were taken three times per device to obtain an average.

The results are shown in figure 9, with the gradient and intercept of the relationship for each device shown in table 1.

Device	Gradient (V/°C)	Intercept (V)
MOSFET 1	-0.002476	0.6567
MOSFET 2	-0.002524	0.6584
MOSFET 3	-0.002582	0.6613
MOSFET 4	-0.002597	0.6609

Table 1: Gradient and Intercept parameters for diode voltage – temperature relationships.

It can be seen that the gradients and intercepts are very similar for all four devices, hence it could be assumed that the gradient and intercept are equal for all the devices.

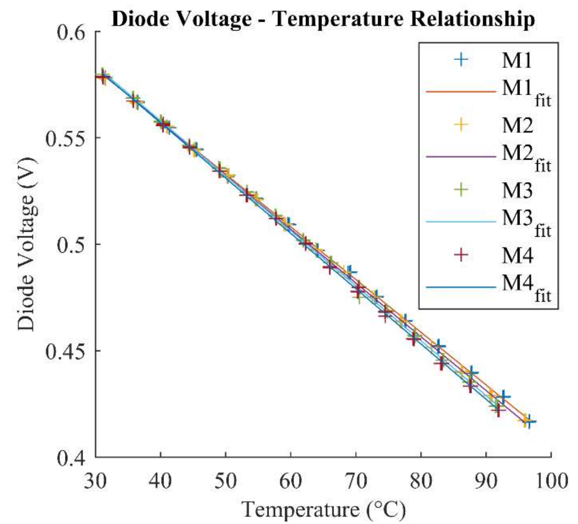

Figure 9: Calibration data and best fit line for each MOSFET device.

However, when tested in the LabVIEW program against the thermocouple readings, the temperatures calculated from the diode voltage were significantly different than expected, with an error of ~10°C when at thermal equilibrium at room temperature. This may have been due to inaccurate calibration data, where the cooling effect of the surrounding ambient air will have resulted in the thermocouple temperatures never truly reaching the die temperature. Furthermore, when observing the calibration experiment using a thermal camera, the hotplate was shown to have an uneven heating effect on the IMS board, with visible hot spots shown in figure 10, which may have contributed to the devices not reaching true thermal equilibrium.

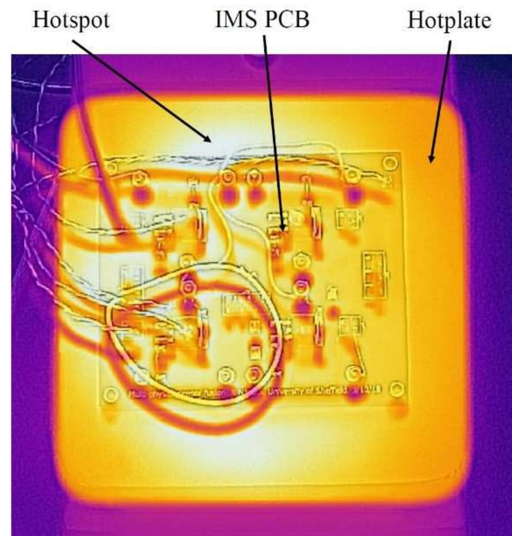

Figure 10: Hotplate hot spots.

Due to all four devices having almost identical calibration parameters, a more precise calibration process was performed on a single device. This was achieved by instead suspending the MOSFET inside a thermally insulating container, which was then placed on top of the hotplate, show in figure 11. In doing this, the MOSFET is not in direct contact with the surface of the hotplate, and the air inside the container is thermally insulated, hence the entire structure of the MOSFET was heated evenly by the surrounding air.

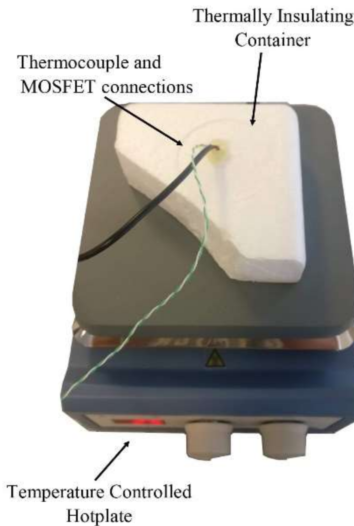

Figure 11: Insulated calibration apparatus.

The results obtained are shown in figure 12 and table 2.

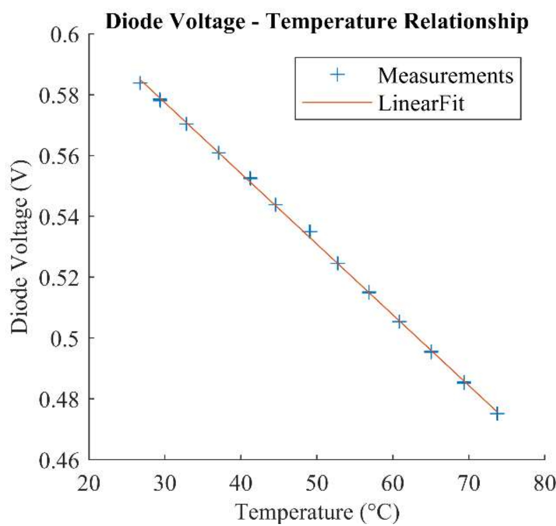

Figure 12: Calibration data and best fit line for single device in thermally insulting container.

Gradient (V/°C)	Intercept (V)
-0.002324	0.6471

Table 2: Gradient and Intercept parameters for the insulated calibration experiment.

The temperatures calculated from the diode voltage measurements using the new calibration data had minimal error at room temperature, typically <1°C when compared to the thermocouple readings. However, as the device was heated, the error between the thermocouple reading and the temperature calculated from the diode voltage increased. This can be explained by the previously mentioned thermal impedance between the semiconductor die and the plastic casing, which according to the devices data sheet is 1°C/W. This was confirmed to be the cause when performing a step dissipation of 10W into a device and observing the thermocouple and die temperatures, which developed a ~10°C error between the two readings at thermal equilibrium as expected, shown in figure 13. This highlights the limitations of using external measurement techniques to measure the temperatures of electronic devices, which if relied on, could result in exceeding safe operating temperatures.

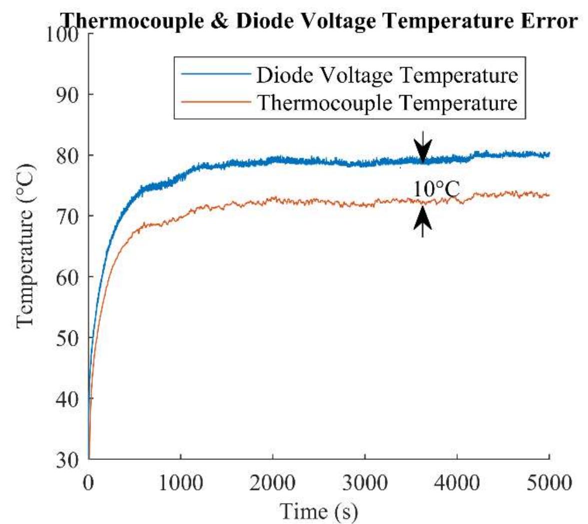

Figure 13: Thermocouple Vs Diode Voltage Temperatures.

Because the temperature error between the thermocouple and voltage measurements was so large at high power dissipations, and the voltage measurement circuit was only able to measure the diode voltage of a single device, the thermal model was developed using thermocouple readings only.

To obtain the step response of the system, a step power dissipation of ~10W was applied to each device in turn, and the temperatures of all four MOSFETs was recorded. This was achieved by using a 2.5Ω power resistor on the power controller circuit, and setting the voltage across the resistor to 5V, resulting in a 10W power dissipation in the MOSFET. The current and voltage across the drain and source of the MOSFET was measured to calculate the exact power dissipation.

The step dissipation was carried out until the temperature of each device reached equilibrium, where the gradient on the LabVIEW graph reached zero. The data was then processed using equation (3) to convert the temperature curve into a transient thermal impedance curve, shown in figure 14 for MOSFET 1.

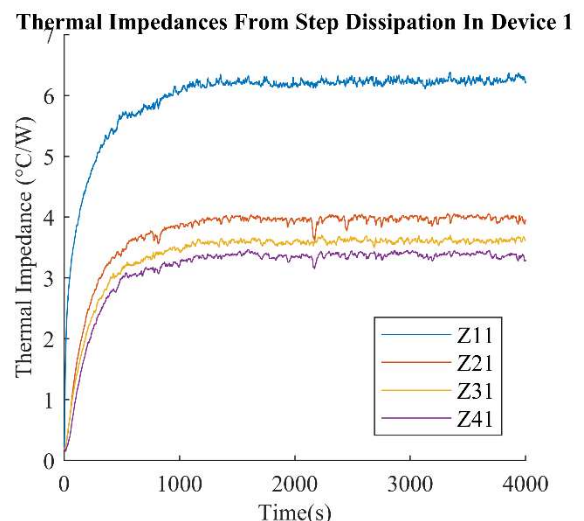

Figure 14: MOSFET 1 Step Response.

As expected, the Z11 thermal impedance is the highest due to the self-heating of MOSFET 1, with Z41 being the lowest due to being the furthest from the heat source on the board.

Theoretically, the thermal impedance curves for Z23 and Z31 should have been identical due to being equidistant from the heat source, but in reality, factors such as mounting bolt locations for the electrical connections and the thermal impedance introduced by the thermal epoxy may have influenced the heat flow.

Once the step dissipation had been performed on all four heat generating devices, the curves were fitted to the multi-term exponential equation so the Foster network RC values could be extracted. Through experimentation, it was found that four exponential terms were sufficient to achieve a suitable curve fit. An example curve fit for Z11 is shown in figure 15.

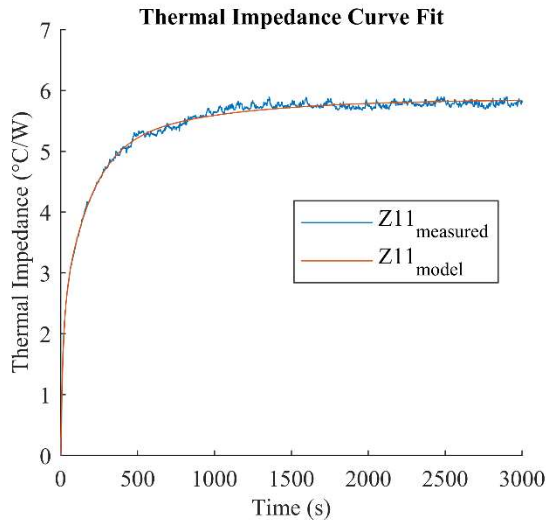

Figure 15: Curve fit of Z11 thermal impedance.

The first exponential term was made negative to take into account the non-instantaneous temperature elevation when the step change in power dissipation is applied. Without making one of the exponential terms negative, the model produced sharp temperature changes as the power dissipation changed, as opposed to curved changes that better resemble real data, shown in figure 16.

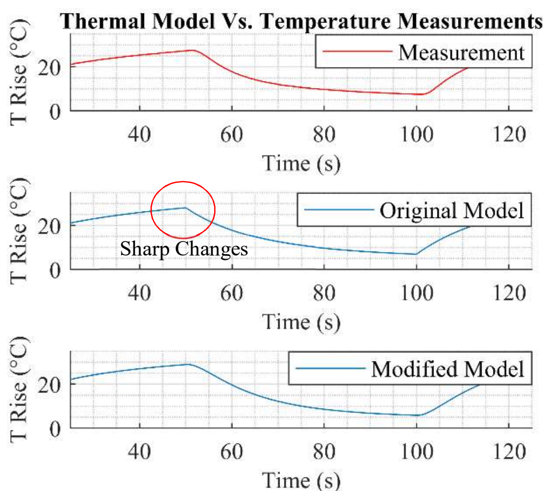

Figure 16: Effects of adding negative coefficient to model.

The RC values obtained for transient thermal impedance Z11 is shown in table 3, with the remaining values shown in Appendix Table 1, and the full RC network is shown in Appendix figure 3.

		Exponential Terms			
		1	**2**	**3**	**4**
Z11	**R**	0.751	3.040	0.501	3.128
	C	3.839	4.185	3629	68.88
Z21	**R**	1.192	3.138	0.720	0.903
	C	8.429	47.04	9.828	610.6
Z31	**R**	1.495	2.709	1.240	0.758
	C	3.818	61.65	3.923	773.9
Z41	**R**	1.603	0.913	3.307	0.381
	C	10.83	12.24	53.56	2728

Table 3: Z11 Thermal Impedance RC values.

To test the model, the transfer function of each RC thermal path using equation (5) was entered into MATLAB with the `tf()` command. The `lsim(Z,P,t)` function was then used for each transfer function `Z` to calculate the temperature elevation of each device due to a given power dissipation `P` in the time domain `t`.

For example, to model the temperature rise of device 1 due to any combination of dissipation in any device, the lsim(Z,P,t) command was used for each transfer function that relates to device 1, shown in (8), Where P1-P4 are the power dissipations of each device in the time domain.

```
T1 = lsim(Z11,P1,t) + lsim(Z12,P2,t) +
lsim(Z13,P3,t) + lsim(Z14,P4,t);     (8)
```

The first tests were performed on device 1, using a square wave generator within the LabVIEW program to generate a dissipation waveform with a variable frequency and duty cycle. The temperature elevation of each device due to a 10W, 10mHz, 50% duty cycle power dissipation in device 1 is shown in Figure 18.

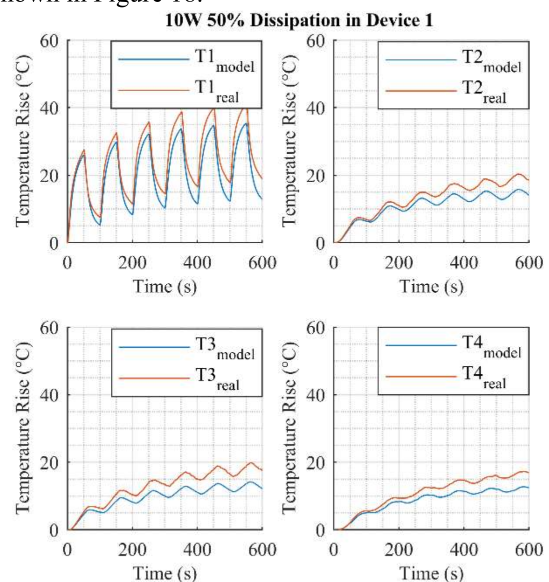

Figure 18: 10W 50% Dissipation in Device 1.

As expected, device 1 has the most dramatic temperature elevation, while T2 and T3 are very similar due to their equal distance from the heat source.

While the model performed well at following the shape of the temperature curves, there is a large error present between the modelled and measured data, with the modelled temperatures being ~6°C lower at steady state. This may have been caused by the model assuming the ambient air temperature was constant, when in reality, due to no forced air cooling, the temperature of the still ambient air surrounding the board would have increased during the experiment. To confirm that this was the cause, the experiment was repeated, shown in figure 19, with an additional thermocouple placed above the board to measure the temperature elevation of the ambient air. A curve fit of ambient air graph was taken and was added to the temperature produced by the existing model.

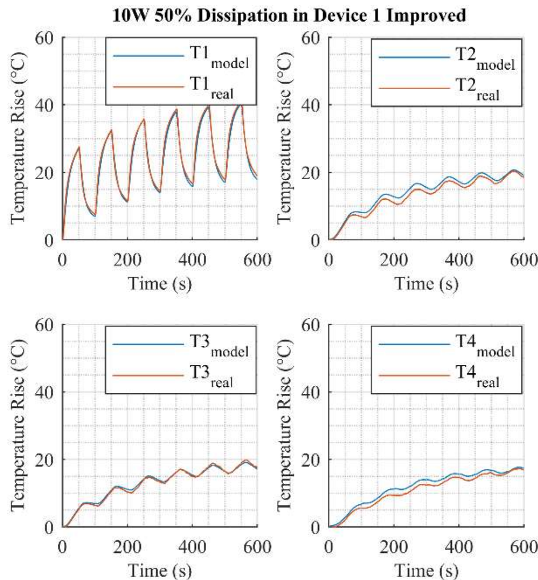

Figure 19: Model improvements from measuring temperature elevation of ambient air.

As seen, the error between the measured and modelled temperature was greatly reduced.

Figure 20 shows the results of a 5W dissipation in both devices 1 & 4 at 10mHz with a duty cycle of 50%.

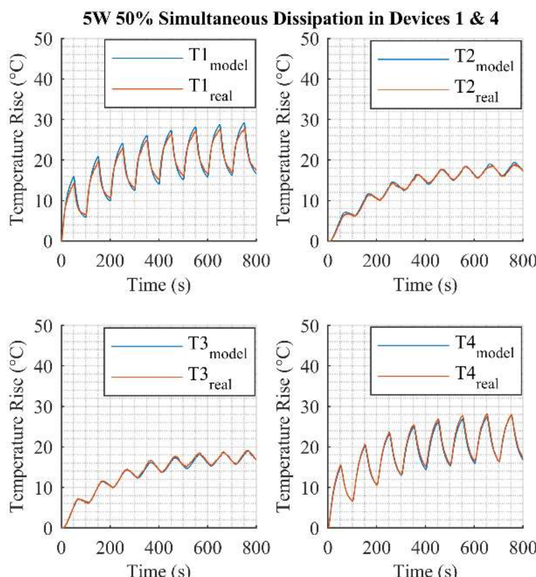

Figure 19: Model vs. measurement results for 5W dissipation in devices 1 & 4.

V. DISCUSSION

By comparing the results shown in figure 19 & 20, the model developed has shown to be capable of predicting the temperature rise of the devices due to both self-heating and thermal cross-coupling with reasonable precision. The errors that remain between the modelled and measured data could be due to subtle ambient temperature fluctuations during the step response experiments. Furthermore, imperfect curve fitting would affect the RC values in the Foster network, leading to small errors in the modelled temperatures. From the results shown in figure 19, the effects of cross coupling were obvious and significant, with a 20°C rise experienced by devices 2-4, despite dissipating no power.

Through exploring temperature measurement techniques, the limitations of external methods were made clear in figure 13, with a 10°C error between the thermocouple reading and the temperature calculated from the diode voltage.

Overall, the majority of the projects initial aims and objectives were met. This included designing a suitable circuit to simultaneously dissipate power in a device and measure its body diode voltage. The board was successfully thermally characterised using its thermal step response, and the Foster network RC values were extracted. Lastly, the transfer functions of each thermal path were modelled, and the completed model was then tested against measured data to assess its accuracy. However, due to time constraints, the model was never tested with an observer. The purpose of the observer would have been to use the additional digital temperatures sensors to correct the temperatures modelled for all the other devices due to changes in operating conditions.

VI. CONCLUSION

The process to thermally characterise a circuit and produce a simple RC model has been presented. Furthermore, a circuit design has been proposed that allows for near simultaneous temperature measurement and power dissipation to obtain a better temperature measurement compared to external methods. The contribution of thermal cross-coupling on a systems overall temperature has been shown, and should be accounted for when designing thermal solutions for an electrical circuit. The thermal model produced is computationally lightweight, meaning that it could be implemented onto a circuit using a microcontroller to monitor devices temperatures and be used in conjunction with other models to determine degradation over time. By implementing this into an electric vehicles power module, the lifetime and reliability of the vehicle's powertrain could be extended, and improved performance could be achieved whilst keeping the devices within their rated operating conditions. This is especially relevant in cases where power modules are packed into tight spaces with limited airflow.

VII. FUTURE WORK

To improve upon the work presented, an Observer would be designed to improve the precision and performance of the thermal model due to unexpected changes in operating conditions.

REFERENCES

[1] M. März, P. Nance, "Thermal Modelling of Power-Electronic Systems," Infineon Technologies, Vishay Siliconix, Munich, Germany, 2000. [Online] Available: https://www.infineon.com/dgdl/Thermal+Modeling.pdf?fileId=db3a30431441fb5d011472fd33c7 0aa3

[2] K.I. Pandya, W. McDaniel, "A simplified method of Generating Thermal Models for Power MOSFETs", CA, USA, 2002. [Online] Available: https://ieeexplore.ieee.org/document/991350

[3] J.N. Davidson, D.A Stone, M.P. Foster, D.T. Gladwin, "Improved Bandwidth and Noise Resilience in Thermal Impedance Spectroscopy by Mixing PRBS Signals," in *IEEE Transactions on Power Electronics, vol. 29, no. 9, pp. 4817.* Sep. 2014. [Online] Available: https://ieeexplore.ieee.org/document/6842658

[4] Z. Zhou, P.M. Holland, P. Igic, "Compact Thermal Model of a Three-Phase IGBT Inverter Power Module," in *26th International Conference on Microelectronics*, Nis, Serbia & Montenegro, June 2008, pp.167-170. [Online] Available: https://ieeexplore.ieee.org/document/4559249

[5] J. Chonko. "Using forward voltage to measure semiconductor junction temperature", Keithley, Aug. 2017. [Online]. Available: https://uk.tek.com/search?keywords=Using%20Forward%20Voltage %20to%20Measure%20Semi conductor%20Junction%20Temperature

[6] J.N. Davidson, D.A Stone, M.P. Foster, D.T. Gladwin, "Measurement and Characterization Technique for Real-Time Die Temperature Prediction of MOSFET-Based Power Electronics," The University of Sheffield. 2015. [Online] Available: https://ieeexplore.ieee.org/document/7239630

[7] M. März, P. Nance, "Thermal Modelling of Power-Electronic Systems," Infineon Technologies, Munich, Germany, 2000. [Online] Available: https://www.infineon.com/dgdl/Thermal+Modeling.pdf?fileId=db3a30431441fb5d011472fd33c70aa3

[8] M.J. Whitehead, C.M. Johnson, "Junction Temperature Elevation as a Results of Thermal Cross Coupling in a Multi-Device Power Electronics Module", in *Electronics System Integration Technology Conference*, Dresden, Germany, 2006, pp. 1218-1223. [Online] Available: https://ieeexplore.ieee.org/abstract/document/4060890

APPENDICES

		Exponential Terms			
		1	**2**	**3**	**4**
Z12	**R**	1.549	0.754	1.167	3.499
	C	5.49	863.9	6.2	48.24
Z22	**R**	2.056	3.542	4	1.151
	C	2.121	42.84	2.469	757.3
Z32	**R**	1.987	0.9943	4.101	0.3925
	C	20.6	41.54	43.07	5275
Z42	**R**	1.047	1.047	1.047	1.047
	C	502.1	502.1	502.1	502.1
Z13	**R**	2.6	1.785	2.759	2.718
	C	11.99	17.46	162.8	45.9
Z23	**R**	3.345	2.561	3.405	1.71
	C	13.67	167.2	36.63	26.75
Z33	**R**	1.2	3.508	3.114	1.898
	C	2.49	120.5	3.142	51.16
Z43	**R**	1.877	2.927	1.03	2.48
	C	15.63	47.11	28.38	176.6
Z14	**R**	2.328	2.119	3.772	0.3714
	C	22.22	191.8	32.97	121.5
Z24	**R**	0.7593	0.5382	9.31E-07	4.239
	C	5.718	5.476	0.004634	62.61
Z34	**R**	2.093	1.68	1.177	3.535
	C	3.818	3.967	464.7	53.09
Z44	**R**	5.215	1.805	7.047	2.935
	C	1.406	315	1.533	50.84

Appendix Table 1: Remaining RC Values.

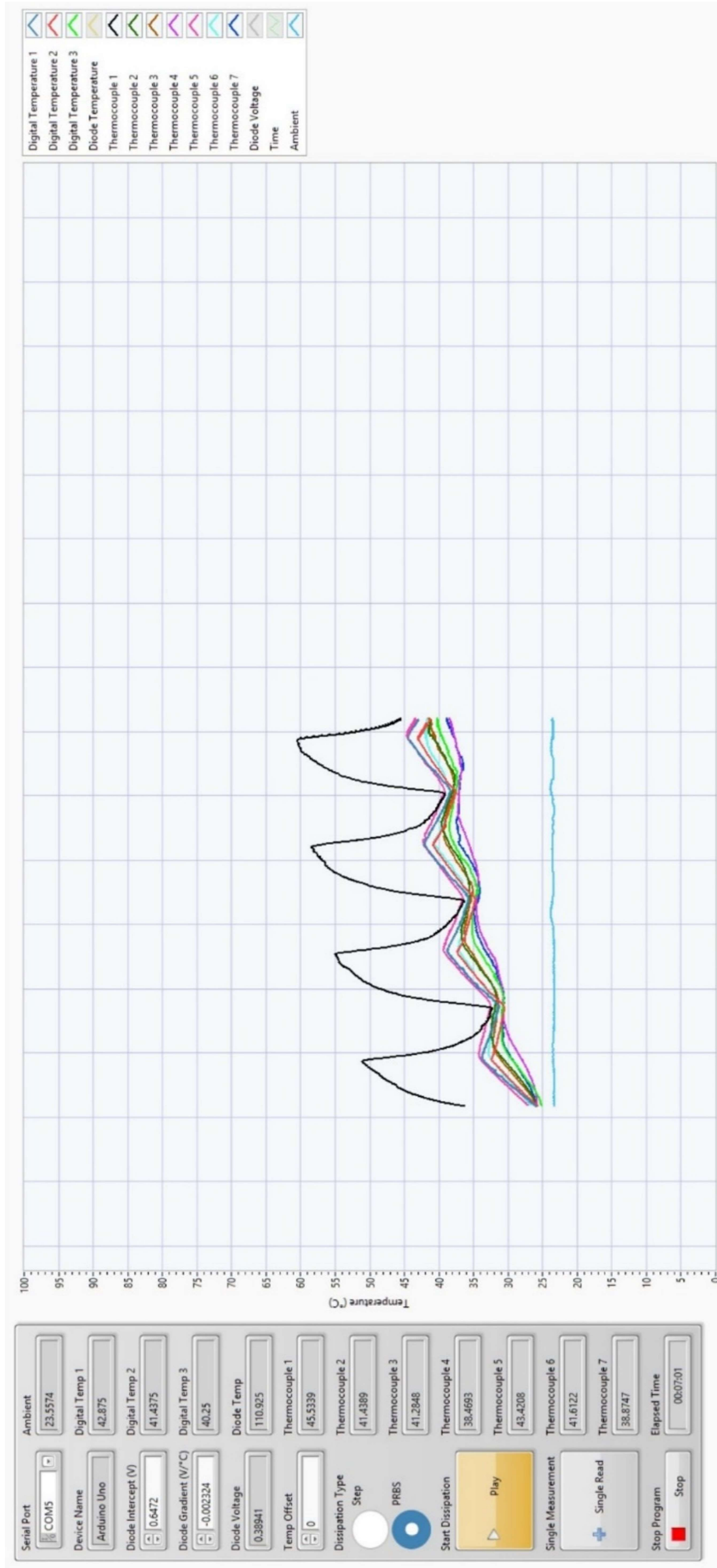

Appendix Figure 1: LabVIEW front panel user interface.

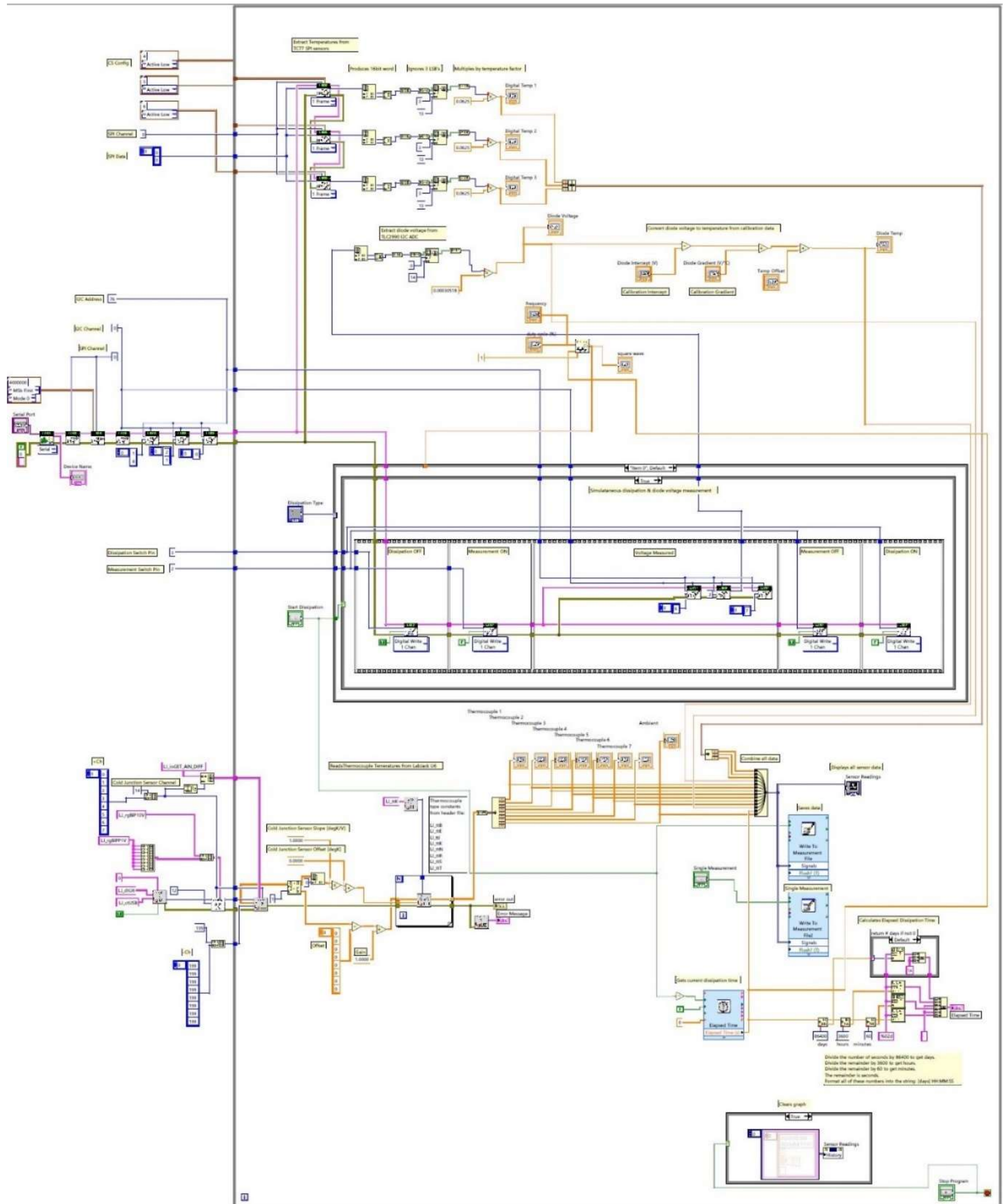

Appendix Figure 2: LabVIEW block diagram.

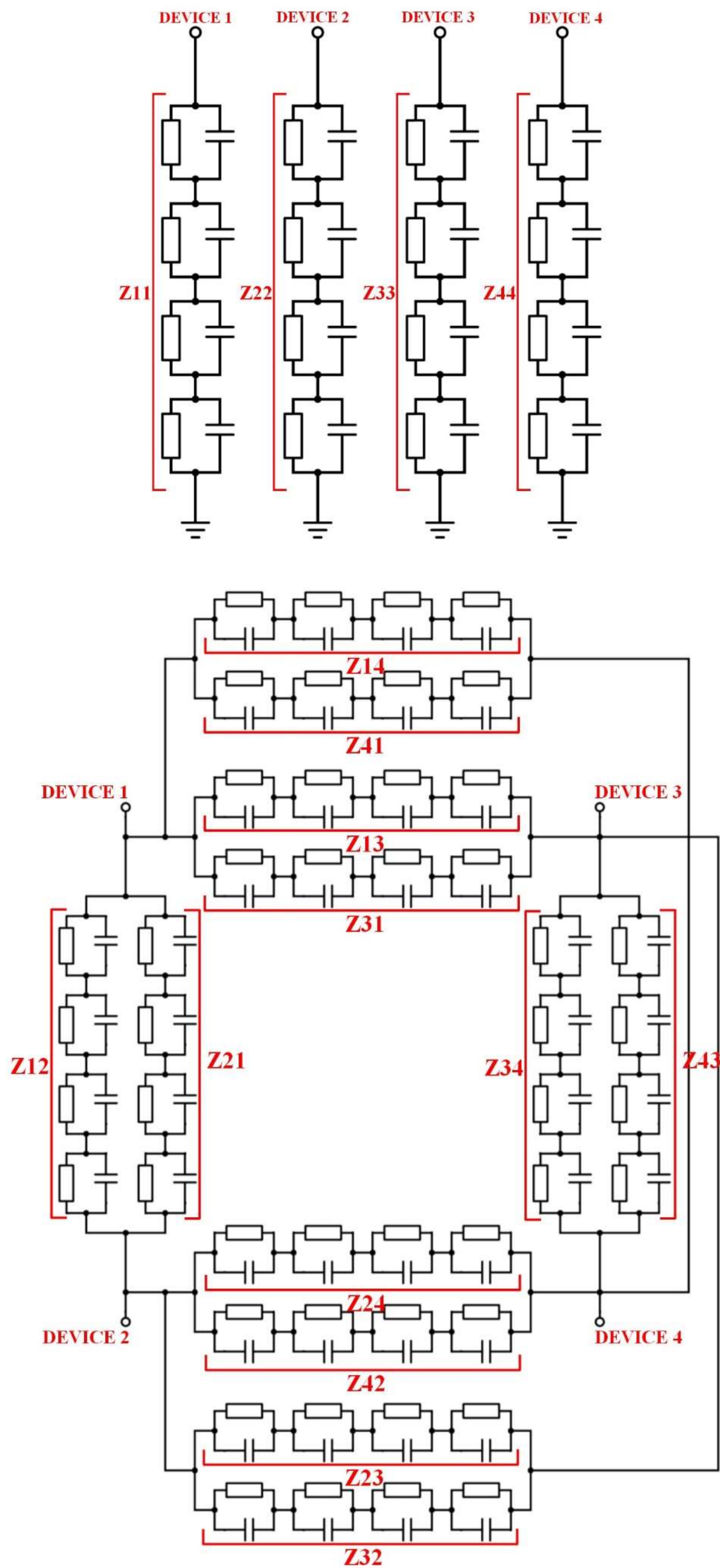

Appendix Figure 3: Foster Network for self-heating (top) and thermal cross coupling (bottom).